Journal of Solid State Chemistry 235 (2016) 113–118

Contents lists available at ScienceDirect

Journal of Solid State Chemistry

journal homepage: www.elsevier.com/locate/jssc

Magnetostructural transition in Fe_5SiB_2 observed with neutron diffraction

Johan Cedervall [a,*], Sofia Kontos [b], Thomas C. Hansen [c], Olivier Balmes [d], Francisco Javier Martinez-Casado [d], Zdenek Matej [d], Premysl Beran [e], Peter Svedlindh [b], Klas Gunnarsson [b], Martin Sahlberg [a]

[a] Department of Chemistry - Ångström Laboratory, Uppsala University, Box 538, 751 21 Uppsala, Sweden
[b] Department of Engineering Sciences, Uppsala University, Box 534, 751 21 Uppsala, Sweden
[c] Institut Laue-Langevin, B.P. 156, 38042 Grenoble Cedex 9, France
[d] MAX IV Laboratory, Lund University, Box 118, 221 00 Lund, Sweden
[e] Nuclear Physics Institute, Academy of Sciences of the Czech Republic, 25068 Rez, Czech Republic

ARTICLE INFO

Article history:
Received 2 October 2015
Received in revised form
10 December 2015
Accepted 12 December 2015
Available online 14 December 2015

Keywords:
Magnetism
X-ray diffraction
Neutron diffraction
Permanent magnet

ABSTRACT

The crystal and magnetic structure of Fe_5SiB_2 has been studied by a combination of X-ray and neutron diffraction. Also, the magnetocrystalline anisotropy energy constant has been estimated from magnetisation measurements. High quality samples have been prepared using high temperature synthesis and subsequent heat treatment protocols. The crystal structure is tetragonal within the space group I4/mcm and the compound behaves ferromagnetically with a Curie temperature of 760 K. At 172 K a spin reorientation occurs in the compound and the magnetic moments go from aligning along the *c*-axis (high *T*) down to the *ab*-plane (low *T*). The magnetocrystalline anisotropy energy constant has been estimated to 0.3 MJ/m^3 at 300 K.

1. Introduction

Magnetic materials, and especially permanent magnets, are of great importance for energy conversion, whether the application comprises energy production or vehicles [1]. The best permanent magnet material known today is the rare earth containing $Nd_2Fe_{14}B$, which was discovered in 1979 [2] with a saturation magnetisation (M_{sat}) of 1.28 MA m^{-1}. Optimisation of the microstructure gave this compound the world record for the energy product ($|BH|_{max}$) with a value of 0.474 MJ/m^3. However, due to high and unstable prices of rare earth elements [3] motivation for research in rare earth free magnetic materials have risen. To manufacture rare earth free permanent magnets, compounds with high amount of 3d-elements should be used.

Magnetism comes from the spin angular momentum of unpaired electrons in the outer shell of transition metals (3d, 4d, 5d) or rare earth elements (4f) [4]. In a rare earth magnet the magnetism comes from the interplay of two different sublattices, one with transition metals and one with rare earths. The 3d elements in a rare earth magnet is what gives the magnet a high Curie temperature (T_C) and high M_{sat}. However, the spin–orbit coupling between the 4f and 3d electrons will give the compound a high magnetocrystalline anisotropy, which potentially gives a high coercivity. In transition metal based magnets the anisotropy comes from the interplay between the crystal field and spin–orbit interactions. The crystal field is given by the 3d electron clouds orientation relative to the crystalline unit cell axis. The spin orbit coupling is dependent on the electrons circular motion.

To find an optimal material for rare earth free permanent magnets one (or several) of the magnetic 3d-elements (Cr, Mn, Fe, Co and Ni) should be present in the material in high concentrations. The 3d-elements will contribute with large and stable magnetic moments and high T_C. However, usually the magnetocrystalline anisotropy energy (MAE) is low in such compounds, resulting in low coercivity in the manufactured magnet giving a soft magnetic material. To overcome the low coercivity, compounds with a uniaxial crystal structure should be used to gain a higher MAE [2]. Examples of this approach are the compounds MnAl and FeNi both crystallising in the $L1_0$ structure, an ordered body centred tetragonal (bct) structure, where the separate atoms are alternating in layers along the *c*-axis [4]. This ordered $L1_0$ phase results in high magnetocrystalline anisotropy, but these structures are often metastable (MnAl) or need extremely slow

* Corresponding author.
E-mail address: johan.cedervall@kemi.uu.se (J. Cedervall).

http://dx.doi.org/10.1016/j.jssc.2015.12.016

cooling (on the order of millions of years) [4] to give local chemical ordering (FeNi). The $L1_0$ phase can be stabilised by for example carbon interstitials in MnAl [5].

One compound that is rich in 3d-elements with a uniaxial crystal structure is the tetragonal compound Fe_5SiB_2 [6] (discovered in 1959), with unit cell parameters 5.5498(2) Å and 10.3324(5) Å for *a* and *c* respectively. Fe_5SiB_2 crystallises in the Cr_5B_3-type structure [6,7], and is isostructural with Fe_5PB_2 within the space group I4/mcm [8]. For Fe_5SiB_2 (as well as for Fe_5PB_2) iron occupies the 16l and 4c sites whereas silicon (phosphorus) and boron occupy the 4a and 8h sites respectively [9]. Fe_5SiB_2 is ferromagnetic at room temperature with a critical temperature at 784(1) K reported from Mössbauer spectroscopy and a suggested magnetisation along the *c*-axis [10]. Mössbauer spectroscopy at low temperatures reveals a change in the easy magnetisation axis at ~140 K [11] where a transition from the *c*-axis to the *ab*-plane for the magnetisation direction is proposed to take place. This can be seen by a non-linear shift in both the electric quadrupole splitting and the hyperfine field, especially for the iron at the 4c position. It has however never been experimentally verified using other methods.

In this study we present direct measurements of the magnetic structures for Fe_5SiB_2 using neutron powder diffraction at high and low temperatures as well as the magnetocrystalline anisotropy energy constant from magnetic measurements; structural parameters were obtained using simultaneous refinement of X-ray and neutron diffraction data.

2. Experimental

2.1. Sample preparation

Samples were synthesised by arc melting stoichiometric amounts of iron (Leico Industries, purity 99.995%. Surface oxides were reduced in H_2-gas), silicon (Highways International, purity 99.999%) and boron (Wacher-Chemie, purity 99.995%) under argon atmosphere. Neutron diffraction samples with isotope ^{11}B (Los Alamos National Laboratories, pure ^{11}B) were also synthesised with arc melting under argon. The synthesis was performed in two steps, first FeB was prepared and second Fe_5SiB_2 was produced from FeB, iron and silicon. The arc melted samples were remelted five times to ensure homogeneity. All samples were crushed, pressed into pellets and heat treated in evacuated silica tubes at 1273 K for 14 days (30 days for the ^{11}B-sample) and subsequently quenched in cold water.

2.2. X-ray powder diffraction

Phase analysis and crystal structure determinations were performed using high resolution X-ray powder diffraction (XRD) obtained at the I711 beamline [12] at the Max II synchrotron of the Max IV laboratory (Lund, Sweden). Samples were measured at the temperature 298 K, in transmission mode in 0.3 mm spinning capillaries, using a Newport diffractometer equipped with a Pilatus 100 K area detector mounted 76.5 cm from the sample ($\lambda = 0.9940$ Å). The detector was scanned continuously, from 5° to 125° in approx. 6–10 min, recording 62.5 images/deg (step size 0.016°) for each measurement. The true 2θ position of each pixel was recalculated, yielding an average number of 100,000 pixels contributing to each 2θ value. Integration, applying no corrections for the tilt of the detector, provided FWHM values of 0.03–0.08° from 5 to 125°. Diffraction patterns were also recorded as a function of temperature with a Bruker D8 diffractometer equipped with a Lynx-eye position sensitive detector (PSD, 4° opening) using CuKα_1 radiation ($\lambda = 1.540598$ Å), in a 2θ range of 20–90°.

2.3. Neutron powder diffraction

Atomic and magnetic structures were determined using neutron powder diffraction at the D1B beamline at ILL (Grenoble, France). A pyrolytic graphite monochromator (reflection 002) was used, giving a wavelength of 2.52 Å. Diffraction patterns were recorded at the discrete temperatures 16, 150, 200, 300 and 500 K and upon ramping between each step with a 2θ range of 5–128°. The sample was kept as an annulus located between the inner and outer walls in a double-walled V container to minimise absorption by the sample.

2.4. Refinement of the crystal and magnetic structures

The X-ray and neutron powder diffraction patterns were analysed with the FullProf software [13] utilizing the Rietveld method [14]. For the X-ray case, the pseudo-Voigt profile function was used to describe the profile function and the background was described by linear interpolation between chosen points. In the refinement the following 18 parameters were varied: zero point, background, scale factor, peak shape, half width parameters (3), unit cell parameters (2), atomic occupancies (4), isotropic temperature parameter and atomic coordinates (5). To precisely determine the unit cell parameters refinements were performed in the software UnitCell [15]. The magnetic structure was described in the Shubnikov groups I4/mc'm' and Iba'm' for 300 and 16 K respectively found from simulated annealing and representational analysis (SARAh) [16]. All Fe atoms were described using the Fe^{3+} form factors.

2.5. Magnetisation

Magnetisation, *M*, measurements were performed using a Quantum Design PPMS 6000 Vibrating Sample Magnetometer (VSM). The low field *M* vs temperature, *T*, dependence was recorded between $T = 950$ K and $T = 10$ K at a constant applied field, *H*, of 40 kA/m. For the range between $T = 950$ K and 305 K, the sample was mounted in the PPMS furnace option, added to the VSM. *M* vs *H* at constant $T = 300$ K and at $T = 10$ K were measured in the range -7.2 MA/m to $+7.2$ MA/m.

3. Results and discussion

3.1. Phase analysis

The XRD investigation confirms that Fe_5SiB_2 crystallises in the tetragonal space group I4/mcm with the refined unit cell parameters $a = 5.5541(1)$, $c = 10.3429(2)$ Å. The diffraction pattern for Fe_5SiB_2 in Fig. 1 shows a nearly single phase diffraction pattern with a small amount (< 2%) of an Fe_3Si secondary phase. From the refined structure model for Fe_5SiB_2 the atomic coordinates and occupancies could be extracted and are shown in Table 1. Fig. 2 shows diffraction patterns from room temperature down to 16 K. The difference in the unit cell parameters comes from lattice contractions due to the decrease in temperature. This shows that the proposed magnetic transition that occurs at ~140 K [11] is only a magnetic transition and is not coupled to a structural transition.

The X-ray diffraction pattern of the sample used for neutron diffraction, $Fe_5Si^{11}B_2$, can be seen in Fig. 3. It is observed that the sample consists of two phases, the primary phase Fe_5SiB_2 (~95%) and a secondary phase $Fe_{4.7}Si_2B$ (~5%). However, the refined unit cell parameters and atomic positions of the majority phase are not different between the two samples.

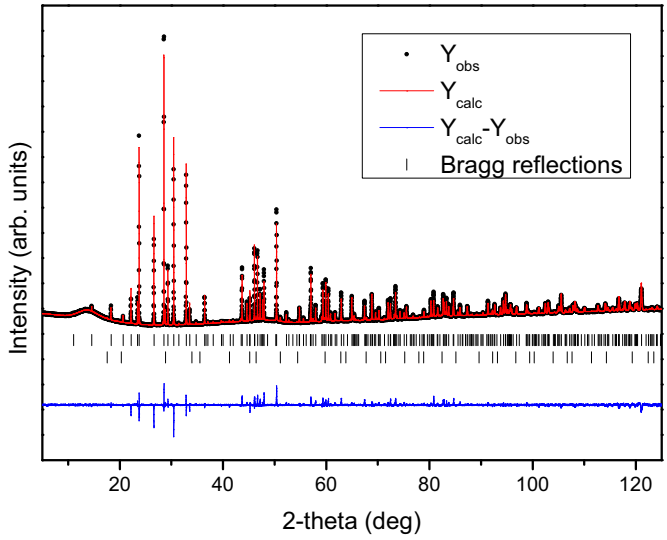

Fig. 1. X-ray powder diffraction pattern of Fe_5SiB_2 refined with the Rietveld method. Black dots and red line correspond to the observed and calculated pattern respectively. Blue line shows difference between observed and calculated data. Bars shows the theoretical Bragg peaks of the Fe_5SiB_2 phase (upper) and the secondary phase, Fe_3Si (lower). $\lambda = 0.9940$ Å. (For interpretation of the references to colour in this figure caption, the reader is referred to the web version of this paper.)

Table 1
Atomic positions and occupancies for Fe_5SiB_2 at room temperature. Derived from high resolution XRD patterns.[a]

Atom	Site	x	y	z	Occ.
Fe1	4c	0	0	0	0.976(8)
Fe2	16l	0.1683(1)	0.6683(1)	0.1384(1)	1
Si	4a	0	0	0.25	1
B	8h	0.6162(9)	0.1162(9)	0	1

[a] Space group: I4/mcm; unit cell parameters: $a = 5.5541(1)$ Å, $c = 10.3429(2)$ Å; Agreement factors: $R_{Bragg} = 9.31$, $R_{wp} = 20.7$; Overall displacement parameter: $B_{iso} = 1.00852$.

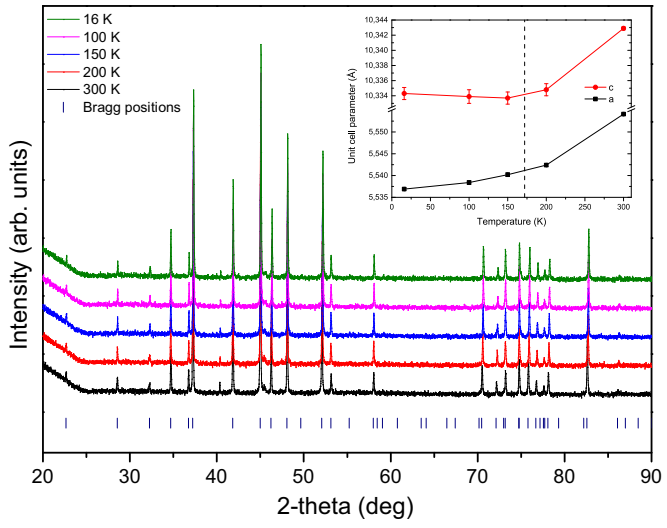

Fig. 2. Temperature dependant XRD patterns for Fe_5SiB_2 showing that no crystallographic structure transition occur around 172 K. Tick marks indicate the Bragg positions for Fe_5SiB_2 at room temperature. Inset shows how the unit cell parameters vary with temperature with the dashed line representing the magnetic transition. $\lambda = 1.540598$ Å.

3.2. Magnetic measurements

M vs *H* for both samples were recorded using VSM technique. The result is shown in Fig. 4 where the different curves correspond to

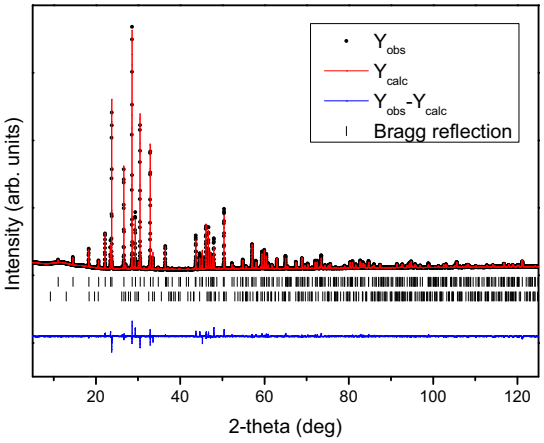

Fig. 3. X-ray powder diffraction pattern of $Fe_5Si^{11}B_2$ refined with the Rietveld method. Black dots and red line corresponds to the observed and calculated pattern respectively. Blue line shows difference between observed and calculated data. Bars shows the theoretical Bragg peaks of the $Fe_5Si^{11}B_2$ phase (upper) and the secondary phase, $Fe_{4.7}Si_2B$ (lower). $\lambda = 0.9940$ Å.

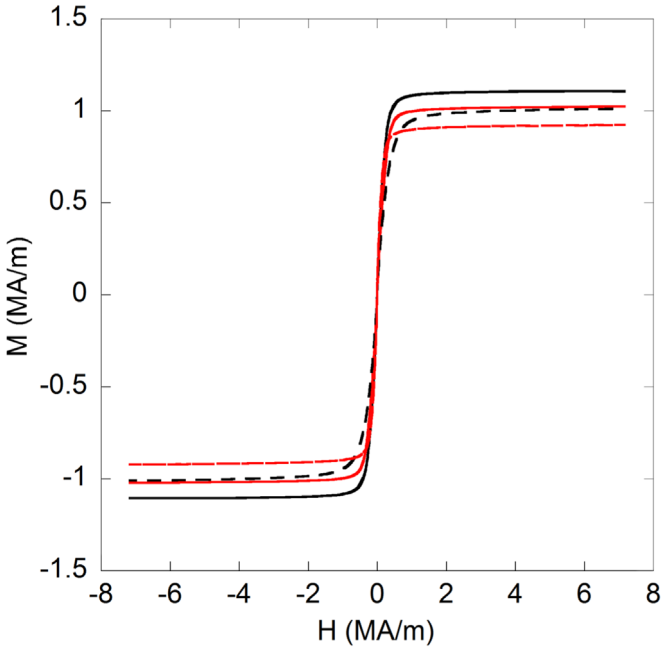

Fig. 4. *M* vs *H*. Top to bottom, Fe_5SiB_2, $T = 10$ K (solid black line) and $T = 300$ K (solid red line); $Fe_5Si^{11}B_2$, $T = 10$ K (dashed black line) and $T = 300$ K (dashed red line). For all samples, the density 6900 kg/m^3 was used for the transformation to SI units. (For interpretation of the references to colour in this figure caption, the reader is referred to the web version of this paper.)

Table 2
Magnetic moments and the anisotropy energy constants for the samples from *M* vs *H* measurements at 10 and 300 K.

Sample	T (K)	M_{sat} (MA/m)	Total magnetic moment (μ_B)	K_1 (MJ/m^3)
Fe_5SiB_2	10	1.10	1.87	0.33
Fe_5SiB_2	300	1.02	1.75	0.30
$Fe_5Si^{11}B_2$	10	1.01	1.72	0.55
$Fe_5Si^{11}B_2$	300	0.92	1.58	0.20

Fe_5SiB_2 (solid line) and $Fe_5Si^{11}B_2$ (dashed line) at $T = 300$ K (red) and $T = 10$ K (black). From Fig. 4, the saturation magnetisation, M_{sat} (defined as *M* at $H = 7.2$ MA/m) is estimated (see Table 2). The magnetic moment per Fe-atom, due to the $Fe_5Si^{11}B_2$ sample in particular, is smaller compared to the results predicted from neutron powder

diffraction. However, according to the XRD results, the Fe_5SiB_2 sample is nearly single phase while $Fe_5Si^{11}B_2$ has higher amounts of a secondary phase. Assuming this phase to be nonmagnetic (or anti-ferromagnetic), it explains, at least to the major extent, the difference in magnetic moment.

Assuming the samples to consist of grains of uniaxial anisotropy, the magnetocrystalline anisotropic energy can be expressed as

$$E_{anis} = K_1 \cos^2\theta + K_2 \cos^4\theta \quad (1)$$

where θ is the angle between the magnetisation and the easy axis of magnetisation and K_1 and K_2 are anisotropic constants. Information relating to the magnetocrystalline anisotropy can be extracted using the so-called law of approach to saturation [17],

$$\frac{M}{M_{sat}} = \left(1 - \frac{b}{H^2}\right), \quad (2)$$

where

$$b = \frac{4}{15}\left(\frac{K_{eff}}{\mu_0 M_{sat}}\right)^2 \quad (3)$$

and defining

$$K_{eff}^2 = K_1^2 + \frac{16}{7}\left(K_1 + \frac{2}{3}K_2\right)K_2 \quad (4)$$

as the effective value of the anisotropic constants [17]. In uniaxial systems, $K_1 > 0$ and $K_2 > -K_1$ and often $K_2 \ll K_1$, e.g. $BaFe_{12}O_{19}$ [18] and $Nd_2Fe_{14}B$ [19]. In these cases, $K_{eff} = K_1$ which then can be estimated from a plot of M vs $1/H^2$ according to the equations above. In case of easy plane anisotropy, either K_1 or K_2, or both, will be negative. Using the law of approach to saturation only, the sign of K_{eff} cannot be extracted. In our case, however, judging from the low temperature neutron data, we can conclude $K_{eff} < 0$ at $T = 10$ K. The magnitude of K_{eff} estimated using the above method is given in Table 2.

In Fig. 5, the $Fe_5Si^{11}B_2$ low field susceptibility $\chi = M/H$ is plotted vs T. The Curie temperature $T_C = 800$ K is estimated from the plot $1/\chi$ vs T

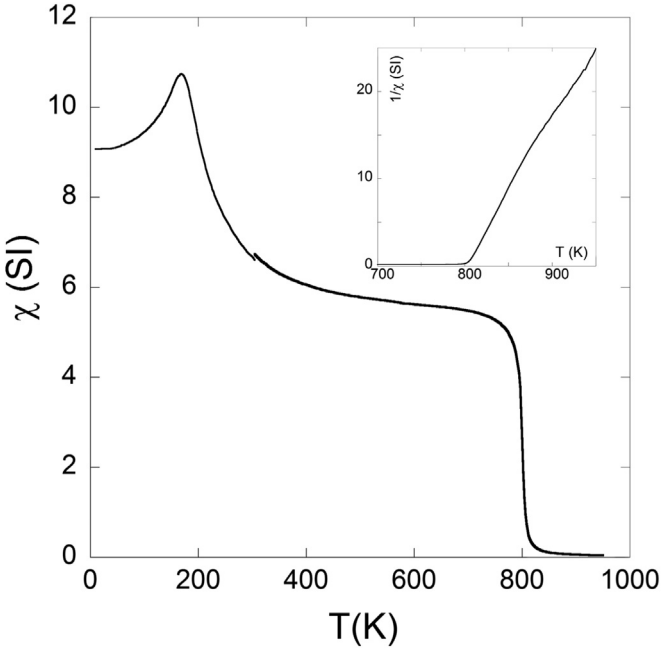

Fig. 5. $Fe_5Si^{11}B_2$ low field susceptibility $\chi = M/H$ vs T at an applied field of $H = 40$ kA/m. The small misfit between the curves (< 2%) is due to loss of sample while changing sample holder between the two setups at $T = 305$ K.

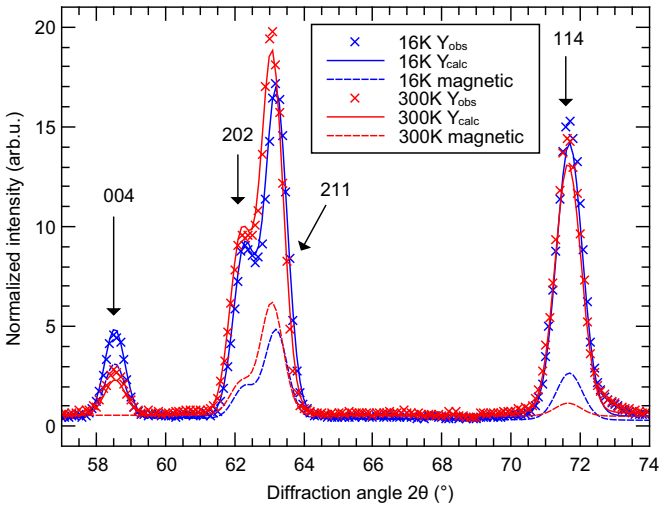

Fig. 6. Neutron powder diffraction patterns revealing the magnetic transition for $Fe_5Si^{11}B_2$. $\lambda = 2.52$ Å.

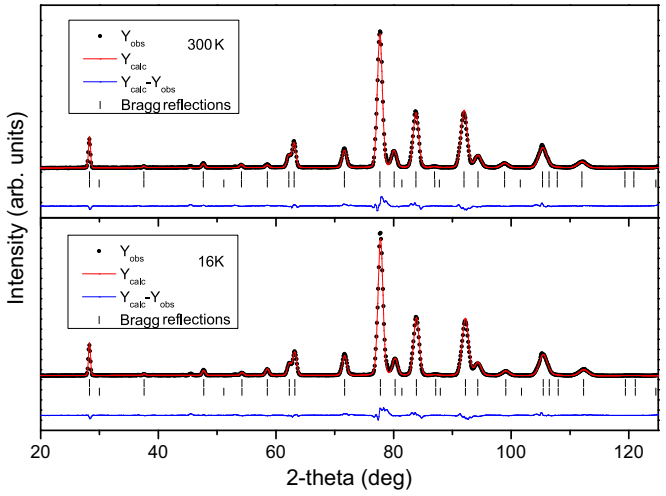

Fig. 7. Neutron powder diffraction patterns of $Fe_5Si^{11}B_2$ refined with the Rietveld method at 300 K (upper) and 16 K (lower). $\lambda = 2.52$ Å.

Table 3
Size and orientation of the magnetic moments for the high and low temperature magnetic structures.

Magnetic atom	Site	x (μ_B)	y (μ_B)	z (μ_B)	Total magnetic moment (μ_B)
High temperature magnetic phase (300 K)					
Fe1	4c	0	0	2.06(7)	2.06(7)
Fe2	16l	0	0	1.72(5)	1.72(5)
$R_{Bragg} = 5.14$, $R_{mag} = 4.90$, $R_{wp} = 9.39$					
Low temperature magnetic phase (16 K)					
Fe1	4c	2.31(6)	0	0	2.31(6)
Fe2	16l	2.10(4)	0	0	2.10(4)
$R_{Bragg} = 4.65$, $R_{mag} = 5.03$, $R_{wp} = 9.72$					

(cf. inset in Fig. 5). At the lower part of the temperature range, there is a pronounced maximum in χ, peaking at $T_t = 169$ K. The χ vs T plot on the Fe_5SiB_2 sample (not shown) yields $T_C = 760$ K and $T_t = 172$ K.

The maximum in $Fe_5Si^{11}B_2$ is indicative of the spin reorientation revealed by the results from neutron powder diffraction. With decreasing temperature, going from the uniaxial to the easy plane state, K_1 (and K_2) will decrease in magnitude, change sign and then increase in magnitude. The zero-crossing in the anisotropic constants is mirrored by the maximum in χ at T_t since the material will be in a

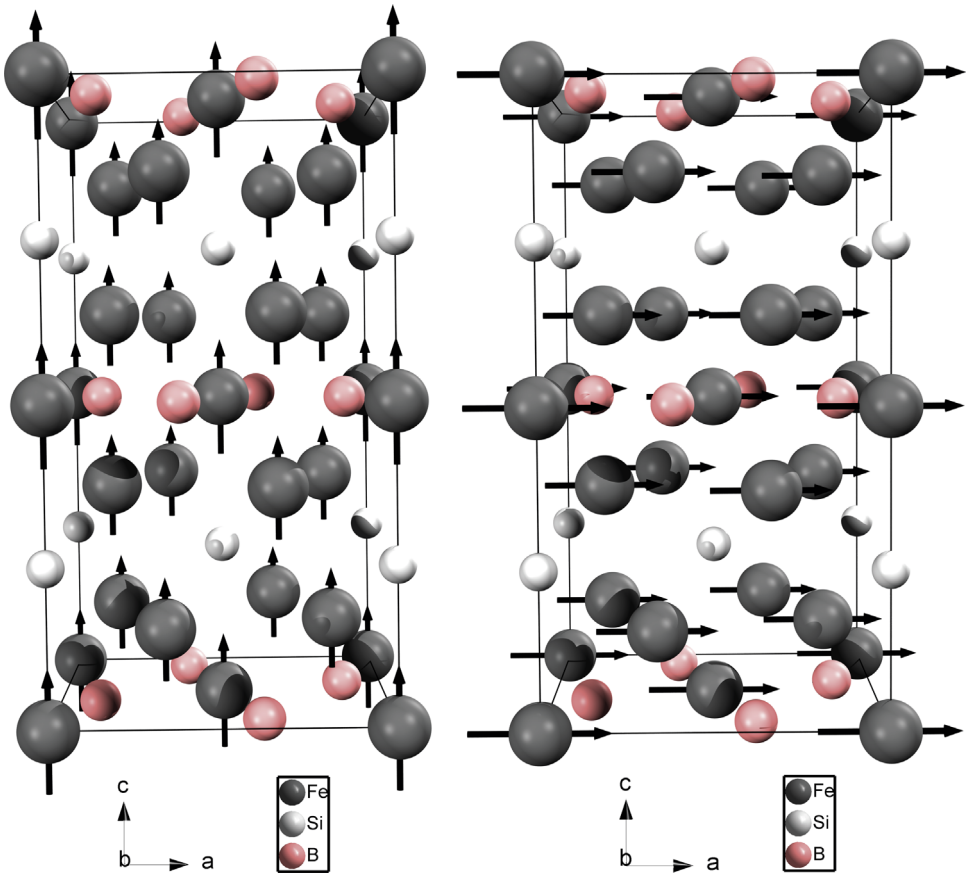

Fig. 8. Magnetic structures for Fe_5SiB_2 at 300 K (left) and 16 K (right). The length of the arrows corresponds with the size of the magnetic moment.

magnetically more soft state. Tentatively speaking, in the easy plane state, the number of easy directions "available" will be larger compared to a uniaxial case and thus the response of the magnetisation to an applied field, i.e. χ, will be larger.

3.3. Magnetic structure

The neutron diffraction patterns show differences above and below the magnetic spin reorientation. Intensities from magnetic scattering at the 004, 211 and 114 peaks are changing with temperature, shown in Fig. 6, indicating a rearrangement in the magnetic structure. All peaks with magnetic contributions to the intensities are at crystallographic peak positions, therefore the magnetic and crystallographic unit cells are the same. This indicates ferromagnetism which is in agreement with the magnetic measurements. The refined neutron powder diffraction patterns can be found in Fig. 7. From the peaks with additional magnetic intensities the direction of the magnetisation is found to be along the *c*-axis at high temperatures and in the *ab*-plane at low temperatures. These proposed magnetic structures (from neutron diffraction) are also in agreement with the magnetic structure model proposed from Mössbauer measurements [11]. The magnetic moment for the high temperature phase has been refined to 2.06(7) μ_B and 1.72(5) μ_B for Fe1 and Fe2 respectively. This gives a mean value for the magnetic moment of 1.79 μ_B which is in good agreement with the value calculated from M_{sat} from the M vs H measurement for the Fe_5SiB_2 sample. For the low temperature phase the moments are 2.31(6) μ_B and 2.10(4) μ_B, see Table 3, giving a mean value of 2.14 μ_B, which is a little higher, but still in agreement with, the corresponding value from M_{sat} for Fe_5SiB_2. The structural models used to refine the neutron powder diffraction patterns for different temperatures are shown in Fig. 8.

4. Conclusions

The magnetic structure of Fe_5SiB_2 has been studied using a combination of X-ray and neutron powder diffraction, and the model proposed from Mössbauer spectroscopy has been verified. The neutron diffraction patterns in combination with magnetic measurements reveal a magnetic structure transition at 172 K where the direction of the magnetisation changes from aligning along the *c*-axis to fall down towards the *ab*-plane upon cooling.

Furthermore, the magnetic properties for permanent magnet applications have been studied. The saturation magnetisation is high, comparable to that of $Nd_2Fe_{14}B$, 1.1 MA/m. However, the magnetocrystalline anisotropy energy is too low for the material to get hard magnetic properties. Therefore, the usefulness as a permanent magnet material is low, although the magnetocrystalline anisotropy could possibly be increased by e.g. substitutions on the iron sites.

Acknowledgements

This work was financed by the Swedish Research Council, which is gratefully acknowledged.

References

[1] O. Gutfleisch, M.A. Willard, E. Brück, C.H. Chen, S.G. Sankar, J.P. Liu, Adv. Mater. 23 (2011) 821–842.
[2] J. Coey, IEEE Trans. Magn. 47 (2011) 4671–4681.
[3] J. Coey, Scr. Mater. 67 (2012) 524–529, Viewpoint Set No. 51: Magnetic Materials for Energy.
[4] R. McCallum, L. Lewis, R. Skomski, I. Kramer, M.J. Anderson, Annu. Rev. Mater. Res. 44 (2014) 451–477.

[5] Q. Zeng, I. Baker, J. Cui, Z. Yan, J. Magn. Magn. Mater. 308 (2007) 214–226.
[6] B. Aronsson, G. Lundgren, Acta Chem. Scand. 13 (1959) 433–441.
[7] B. Aronsson, I. Engström, Acta Chem. Scand. 14 (1960) 1403–1413.
[8] S. Rundqvist, Acta Chem. Scand. 16 (1962) 1–19.
[9] L. Häggström, R. Wäppling, T. Ericsson, Y. Andersson, S. Rundqvist, J. Solid State Chem. 13 (1975) 84–91.
[10] R. Wäppling, T. Ericsson, L. Häggström, Y. Andersson, J. Phys. Colloq. 37 (1976) 591–593.
[11] T. Ericsson, L. Häggström, R. Wäppling, Phys. Scr. 17 (1978) 83.
[12] Y. Cerenius, K. Ståhl, L.A. Svensson, T. Ursby, Å. Oskarsson, J. Albertsson, A. Liljas, J. Synchrotron Radiat. 7 (2000) 203–208.
[13] J. Rodriguez-Carvajal, Physica B: Condens. Matter 192 (1993) 55–69.
[14] H.M. Rietveld, J. Appl. Crystallogr. 2 (1969) 65–71.
[15] T.J.B. Holland, S.A.T. Redfern, Mineral. Mag. 61 (1997) 65–77.
[16] A. Wills, Physica B: Condens. Matter 276–278 (2000) 680–681.
[17] S. Andreev, M. Bartashevich, V. Pushkarsky, V. Maltsev, L. Pamyatnykh, E. Tarasov, N. Kudrevatykh, T. Goto, J. Alloys Compd. 260 (1997) 196–200.
[18] J.J. Went, G.W. Rathenau, E.W. Gorter, G.W. van Oosterhout, Philips Technical Review, v. 13–14, Philips Research Laboratory, 1952.
[19] T. Schrefl, H. Roitner, J. Fidler, J. Appl. Phys. 81 (1997) 5567–5569.